



Published in final edited form as:

*Oncogene*. 2020 May ; 39(20): 3965–3979. doi:10.1038/s41388-020-1269-5.

## CBX7 binds the E-box to inhibit TWIST-1 function and inhibit tumorigenicity and metastatic potential

Juanni Li<sup>1</sup>, Ayesha B. Alvero<sup>2</sup>, Sudhakar Nuti<sup>2</sup>, Roslyn Tedja<sup>2</sup>, Cai M. Roberts<sup>2</sup>, Mary Pitruzzello<sup>2</sup>, Yimin Li<sup>1</sup>, Qing Xiao<sup>1</sup>, Sai Zhang<sup>1</sup>, Yaqi Gan<sup>1</sup>, Xiaoying Wu<sup>1</sup>, Gil Mor<sup>2,3</sup>, Gang Yin<sup>1</sup>

<sup>1</sup>Department of Pathology, Xiangya Hospital, School of Basic Medical Sciences, Central South University, Changsha, Hunan Province, China

<sup>2</sup>Department of Obstetrics, Gynecology and Reproductive Sciences, Division of Reproductive Sciences, Yale School of Medicine, New Haven, CT, USA

<sup>3</sup>C.S. Mott Center for Human Growth and Development, Department of Obstetrics and Gynecology, Wayne State University, Detroit, MI, USA

### Abstract

Deaths from ovarian cancer usually occur when patients succumb to overwhelmingly numerous and widespread micrometastasis. Whereas epithelial-mesenchymal transition is required for epithelial ovarian cancer cells to acquire metastatic potential, the cellular phenotype at secondary sites and the mechanisms required for the establishment of metastatic tumors are not fully determined. Using *in vitro* and *in vivo* models we show that secondary epithelial ovarian cancer cells (sEOC) do not fully re-acquire the molecular signature of the primary epithelial ovarian cancer cells from which they are derived. Despite displaying an epithelial morphology, sEOC maintains a high expression of the mesenchymal effector, TWIST-1. TWIST-1 is however transcriptionally non-functional in these cells as it is precluded from binding its E-box by the PcG protein, CBX7. Deletion of CBX7 in sEOC was sufficient to reactivate TWIST-1-induced transcription, prompt mesenchymal transformation, and enhanced tumorigenicity *in vivo*. This regulation allows secondary tumors to achieve an epithelial morphology while conferring the advantage of prompt reversal to a mesenchymal phenotype upon perturbation of CBX7. We also describe a sub-classification of ovarian tumors based on CBX7 and TWIST-1 expression, which predicts clinical outcomes and patient prognosis.

Users may view, print, copy, and download text and data-mine the content in such documents, for the purposes of academic research, subject always to the full Conditions of use:[http://www.nature.com/authors/editorial\\_policies/license.html#terms](http://www.nature.com/authors/editorial_policies/license.html#terms)

**Corresponding Authors:** Gil Mor, MD, PhD, Department of Obstetrics and Gynecology, Wayne State University, 275 E. Hancock St., Detroit, MI 48201 USA, [gmor@med.wayne.edu](mailto:gmor@med.wayne.edu) Gang Yin, PhD, School of Basic Medicine, Central South University, 172 TongZiPo Rd. Changsha, Hunan, China 410013, [gang.yin@csu.edu.cn](mailto:gang.yin@csu.edu.cn).

**Author contributions:** JL, performance of experiments, data collection, data analysis, writing of manuscript; AA, design of experiment, development of experimental model systems, data analysis and interpretation, writing and editing manuscript; SN, RT, CR, MP, YL, QX, SZ, YG, performance of experiments, data collection, data analysis; GM and GY, conception, design of experiment, development of experimental model systems, data analysis and interpretation, writing and editing manuscript. The authors do not have any conflict of interest to declare.

## Keywords

ovarian cancer; metastasis; epithelial-mesenchymal transition; mesenchymal-epithelial transition

---

## Introduction

Epithelial ovarian cancer (EOC) is the most lethal of all gynecologic malignancies and accounts for more deaths than cervical and endometrial cancers combined [1, 2] [3]. Mortality in ovarian cancer occurs in part due to failures in early detection and in part due to the lack of effective modalities that can combat the combined occurrence of chemoresistance and carcinomatosis, which persistently develop during disease progression [4] [2, 5, 6].

Unlike other solid cancers, which metastasize via the hematogenous route and give rise to discrete foci of secondary tumor implants, ovarian cancer metastasizes via the transcoelomic route [7, 8] and yield overwhelmingly numerous and widely spread micrometastases distributed throughout the peritoneal cavity [9]. This clinical presentation significantly impacts the success of treatment as it limits the value of debulking surgery consequently contributing to patient mortality.

Being epithelial in nature, metastasis in solid cancers (such as ovarian) requires the process of epithelial-mesenchymal transition (EMT) wherein non-migratory epithelial cancer cells reorganize their cytoskeletal and adhesion molecules and activate pro-survival pathways leading to anoikis resistance and the acquisition of a mesenchymal and migratory phenotype [10, 11]. In ovarian cancer, these mesenchymal cells are carried passively around the abdominal cavity by the peritoneal fluid before attaching to their preferential “soil”, the mesothelium [12, 13]. Upon attachment, cells undergo the reverse process of mesenchymal-epithelial transition (MET) giving rise to secondary epithelial ovarian cancer cells (sEOC) and establish tumors on secondary sites[14]. sEOC are characterized by the re-acquisition of epithelial morphology and a more proliferative phenotype that supports the progression of metastatic disease [15, 16]. MET is therefore considered a critical step in the formation of secondary implants and is a final step in metastasis formation. In theory, the secondary sites can also be a source of metastatic cells that would allow further tumor expansion leading to generalized carcinomatosis, which are typically observed in patients. This process may require the reactivation of EMT in the sEOC in order to generate these additional metastatic sites [17, 18] However, since the nature of the ovarian cancer cells in the secondary metastatic sites is yet to be fully characterized, it is not clear if MET does occur in ovarian cancer during metastasis formation. In addition, it remains to be determined if sEOC would require repetitive EMT to generate additional metastatic sites. Its elucidation is a markedly important step in the identification of effectors that can be targeted in the quest to develop better therapeutic strategies to curtail metastatic tumor burden and improve patient survival.

The characteristic loss of intercellular adhesions, gain of cell motility, and increased invasive activity observed during EMT are driven by the activation of several transcription factors, which include members of the Snail (SNAI1 and SNAI2)[19, 20], Twist (TWIST1 and TWIST2) [21–23] and ZEB families of protein (ZEB1/DEF1 and ZEB2/SIP1) [16, 24–27]. The reverse process of MET is thought to be associated with the repression of these factors,

allowing the re-expression of intercellular adhesion molecules, loss of cell motility and acquisition of the epithelial phenotype [18, 28, 29]. The activation/inhibition of these transcription factors, which control EMT/MET is regulated by multiple mechanisms such as gene mutations, hypermethylations, and promoter repression [18, 30].

An important group of proteins controlling cell fate during development is the polycomb group of proteins (PcG) that make up the Polycomb repressive complex 1 (PRC1) and Polycomb repressive complex 2 (PRC). These complexes function as epigenetic regulators in both normal and pathogenic conditions by silencing key genes that control cell fate and differentiation [31–34]. Several studies suggest that PcG proteins play a role in EMT but its function in MET is still poorly understood. This is especially true in the context of ovarian cancer.

To this end we developed *in vitro* and *in vivo* models of MET that would allow us to determine the epithelial/mesenchymal nature of the sEOC that arise at the metastatic sites and identify drivers that promote the unique characteristics of the micrometastases observed in ovarian cancer patients. In this study we demonstrate that at the metastatic sites, the sEOC that arise do re-acquire an epithelial morphology. However, contrary to previously thought, the sEOC generated are molecularly distinct from the primary epithelial ovarian cancer cells from which they were derived. sEOC, despite its epithelial morphology, are characterized by the maintenance of TWIST-1 expression, which is a classical effector of the mesenchymal phenotype. Interestingly, our data demonstrate that the epithelial morphology of the sEOC is achieved by blocking TWIST-1 activity instead of down-regulating TWIST-1 expression. We demonstrate that the PcG protein CBX7, is sufficient to block TWIST-1 function and impacts the EMT/MET phenotype, tumorigenicity, and metastatic potential of the sEOC. The ability of CBX7 to block TWIST-1 function allows the maintenance of TWIST-1 expression, hence a mesenchymal molecular phenotype, while achieving an epithelial morphology. Additionally, we demonstrate that TWIST-1 and CBX7 expression can be used as prognostic markers for ovarian cancer patients.

## Materials and Methods

### Cell lines, culture conditions, and generation of spheroids and sEOC

Three epithelial ovarian cancer cell lines were used: R182, R2615, and OVCAR3. OVCAR3 was purchased from ATCC. R182 and R2615 were isolated from ascites obtained from patients diagnosed with stage III/IV serous ovarian carcinoma and their characterization has been previously reported by our group [35–40]. Similarly, the isolation and characterization of mCherry+ OCSC1-F2 ovarian cancer cell line have been previously described [41–44]. STR profiling was performed every year and mycoplasma testing was performed every month. In this study, these three cell lines are designated as “primary” epithelial ovarian cancer cells. The ovarian cancer cell lines R182 and R2615 have been previously described by our group as negative for TWIST-1 [40] and the epithelial markers they express are shown in Supp. Fig. 1. All patients signed consent forms and the use of patient samples was approved by Yale University’s Human Investigations Committee (HIC no. 10425). Cells were grown in RPMI media supplemented with 10% FBS, 1000 U/ml penicillin, 100 ug/ml

streptomycin, 10 mM HEPES, 100 nM non-essential amino acids, and 1mM sodium pyruvate and cultured at 37°C with 5% CO<sub>2</sub>.

3D spheroids were derived from the primary epithelial ovarian cancer cells as previously described [45]. Briefly, cells were maintained in high confluence in low-serum conditions (1% fetal bovine serum) until multiple foci undergo morphological changes to a fibroblastic phenotype (Supp. Fig. 2), typically after two weeks in culture. Media collection followed by centrifugation isolated cells that have detached. Cell pellets were re-suspended in growth media and cultured in ultra-low attachment plates (Corning Life Sciences, Corning, NY) for 5 days to promote spheroid formation. The resulting spheroids are typically not uniform in size but exhibit a compacted morphology with a distinct outer layer. Without any further selection, 5-day old spheroids were transferred to tissue culture-treated flasks, allowed to re-attach, and passaged 5 times. The resulting sEOC at p5 to p10 were used for the experiments.

### Plasmid transfection

Cells were transfected using FuGENE 6 Transfection Reagent (Roche Diagnostics, Indianapolis, IN) according to the manufacturer's instructions. For transient transfection, transfected cells were grown for 48 h before RNA or proteins were extracted. For stable transfection, transfected cells were selected by treatment with 1 µg/mL puromycin. shCBX7 plasmid was a gift from Dr. Tom Kerppola, University of Michigan Medical School, Ann Arbor, MI. pCDNA-TWIST-1 was a gift from Dr. Carlotta Glackin, City of Hope, Duarte, CA. pGL3 was a gift from Dr. Xiaoyong Yang, Yale University, New Haven, CT. The miR-199A promoter sequence was obtained by PCR amplification from total cDNA from sEOC and was cloned into pGL3. The primers for the miR-199A promoter used for vector construction are shown in Supplementary Table 1.

### Quantification of mir-199A promoter activity

$5 \times 10^5$  cells were seeded in 6-well plates and transfected with 800 ng of pGL3-miR-199a [46] with or without CBX7 and/or TWIST-1 plasmid. 48 h after transfection, cell extracts were prepared and luciferase activity quantified using the Dual Luciferase Reporter Assay Kit (Promega, Madison, WI, USA). The pRL-TK vector expressing Renilla gene was used to normalize transfection efficiency. For all transfections, the total amount of transfected DNA was equilibrated with the empty vector.

### RNA extraction and qRT-PCR analysis

Total RNA was extracted using either the RNeasy Mini kit (Qiagen, Valencia, CA) or TRIZOL reagent (Invitrogen, Thermo Fisher Scientific, Waltham, MA). 1 µg of RNA was reverse transcribed to cDNA using first-strand cDNA synthesis kit (Invitrogen) for mRNA or Ncode miRNA first-strand cDNA synthesis kit (Invitrogen). cDNA at 1:10 dilution was used for each PCR reaction with appropriate primers using Real-Time SYBR Green/Rox PCR supermix (Invitrogen). All PCR reactions were performed on CFX96- Real-Time System (Bio-Rad, Hercules, CA) in triplicates and validated by the presence of a single peak in the melt curve analysis. GAPDH or NRU6B was used as reference gene. Relative expression

was calculated using the  $2^{-Ct}$  method. Primer sequences are listed in Supplementary Table 1.

### RNA sequencing and enrichment analysis

Total cellular RNA was prepared using TRIZOL reagent and used as input. The RNA-seq library was enriched using KAPA mRNA HyperPrep Kit (KAPA Biosystem, Wilmington, MA). The multiplex library was then subjected to high-throughput sequencing using HiSeq 4000 platforms (Illumina) at Yale Center for Genome Analysis. Differential expression analysis was conducted using limma R package. Raw counts were normalized using “limma-trend” approach. Differentially expressed genes were identified by treating group as a fixed effect variable and subjects as a random effect variable.

### Protein extraction and quantification

Protein extraction was carried out as previously described [37, 47]. Protein samples were quantified using Pierce™ BCA protein assay kit (Thermo Fisher Scientific) according to manufacturer's instructions.

### SDS polyacrylamide gel electrophoresis and western blot analysis

Protein samples were denatured in sample buffer and subjected to 12% SDS–polyacrylamide gel as previously described [39, 48]. Protein was transferred to PVDF membranes and the blots were developed using enhanced chemiluminescence (NEN Life Sciences, Waltham, MA) and imaged using Kodak 20000MM Image Station.

Antibodies were diluted as follows: anti-CBX7 (1:1000, no. 21873, Abcam, Cambridge, MA), anti-TWIST-1 (1:200, no. 81417; Santa Cruz Biotechnology, CA), anti-Slug (1:1000, no. 9585; Cell Signaling Technology, Danvers, MA), anti-FOXC2 (1:1000, no. 12974; Cell Signaling Technology, Danvers, MA), anti-β-actin (1:10000, KM9001; Sungene Biotech, Tianjin, China) and anti-GAPDH (1:1000, Sigma-Aldrich, Cell Signaling Technology, Danvers, MA).

### Chromatin-immunoprecipitation and PCR

Chromatin immunoprecipitation (ChIP) was performed as previously described [49]. Anti-CBX7 antibody (ab21873, abcam, Cambridge, MA, USA) was added to the test groups rabbit IgG (sc-2027, Santa Cruz Biotechnology, Dallas, TX, USA) was used as control. Quantitative PCR (qPCR) primer sequences are listed in Supplementary Table 1. GAPDH primers were used negative control.

### Immunoprecipitation

500 ug of total protein was used for immunoprecipitation (IP) using anti-CBX7 or anti-TWIST (both at 1:100 dilution). Rabbit IgG or mouse IgG were used as controls. After an overnight incubation, the IP product was isolated using Protein-A-Sepharose beads (Life technologies, Carlsbad, CA).

## KO of CBX7 and TWIST-1 using CRISPR/Cas9

CBX7 was KO in sEOC using protocols that were previously described [48]. Briefly, the guide RNAs (gRNAs) were designed using CRISPR design tool (<http://guides.sanjanalab.org>). gRNA sequences for CBX7 are: AGAGAGGTCCGAAACCCAAG (sg1) and TCTCCTCGTAGGCCATGACG (sg4). These gRNAs were introduced to lentiCRISPRv2 plasmid. 10 µg of the resulting plasmid was co-transfected with 8 µg packaging plasmid (pVSVg) and 4 µg envelope plasmid (psPAX2) in the presence of 60 µg PEI on HEK293T cells in 100mm dish. The packaged plasmids were collected and transduced into the sEOC cells.

TWIST-1 was KO in mCherry+ OCSC1-F2 [41, 42, 48, 50]. TWIST-1 guides were designed using the CRISPR design tool (crispr.mit.edu). Due to predicted off target effects, a double nickase approach was selected. Two sets of complementary oligos were hybridized and each hybrid pair was cloned into the PX462 vector. pSpCas9n(BB)-2A-Puro (PX462) V2.0 was a gift from Feng Zhang (Addgene plasmid # 62987 ; <http://n2t.net/addgene:62987> ; RRID:Addgene\_62987) [51]. Oligos were: 1F, 5'-CACCGGGCCGGCGAGACTGGCGAGC-3'; 1R, 5'-AAACGCTCGCCAGTCTCGCCGG-CCC-3'; 2F, 5'-CACCGCGACAGCCTGAGCAACAGCG-3'; 2R, 5'-AAACCGCTGTTGCTCAGGCTGTCGC-3'. Following sequence verification, the full U6-gRNA cassette was PCR amplified from one vector and cloned into the other to create a single vector with both gRNAs expressed. 5 µg of this final plasmid was mixed with 15 µl of XtremeGene 9 (Sigma Aldrich, St. Louis, MO) and added to F2 cells in suspension in a T25 flask. Knockout cells were selected by growth in puromycin.

## Mouse xenograft studies

The Yale University Institutional Animal Care and Use Committee and the Animal Care and Use Committee at Central South University approved the *in vivo* studies described. Sample size is based on statistical analysis of variance and on prior experience with specific experimental setup. Human ovarian cancer xenografts were established in 4–6 week old female athymic nude mice. For studies involving spheroids, 100 µl packed volume of pelleted spheroids were re-suspended in 200 µl of RPMI supplemented with 10% FBS and injected either sub-cutaneously (s.c.) or intra-peritoneally (i.p.) using a 26G needle. For studies involving knock-out (KO) cells, mice were randomly assigned to control or experimental groups (n=6 per group).  $3 \times 10^6$  cells were resuspended in 200 µl of growth media and injected i.p. Depending on the study, animals were euthanized between 3 to 8 weeks and resulting tumors were dissected and snap frozen in liquid nitrogen or fixed in 4% paraformaldehyde for further analysis. No inclusion/exclusion criteria were used. All animals were included in the analysis. Investigators were not blinded during data acquisition and analysis.

## Patient samples

Written informed consent was obtained from all patients prior to the study. The Ethics Review Committee of The Affiliated Cancer Hospital of XiangYa School of Medicine and the Ethics Review Committee of Xiangya Hospital of Central South University approved the use of patient samples. The 211 paraffin-embedded archived ovarian cancer tissues used in

this study were histopathologically and clinically diagnosed at the Xiangya Hospital and the Affiliated Cancer Hospital of XiangYa School of Medicine between 2008 and 2012. The tumors were obtained from the primary site (ovarian tumor). Supplementary Table 2 shows patient demographics and clinical information. All samples were obtained from newly diagnosed patients and from the ovarian primary site.

### Immunohistochemistry

Tissue sections were deparaffinized and rehydrated in ethanol. Antigen retrieval was performed in a pressure cooker using Tris-EDTA (pH=8.0). Endogenous peroxidase activity was blocked with 1% hydrogen peroxide for 20 min. Slides were incubated overnight at 4°C with antibody against TWIST-1 (1:150; no. 81417; Santa Cruz Biotechnology, CA) or with antibody against CBX7 (1:50; no. 21873, Abcam, Cambridge, MA) followed by incubation with labeled polymer-HRP solution for 30 min. Staining was developed using 3,3'-Diaminobenzidine according to the manufacturer's instructions. Nuclei were stained with hematoxylin. Staining was analyzed by two pathologists and scored by evaluating both the staining intensity and percentage of positive cells.

### Statistical analysis

Sample size is based on statistical analysis of variance and on prior experience with specific experimental setup. All data are presented as mean  $\pm$  SEM. Data were analyzed using unpaired t test when analyzing two groups or Ordinary One-way ANOVA followed by *post hoc* analysis when analyzing multiple groups.  $p < 0.05$  was considered as statistically significant. Data were graphed and analyzed using Prism Graph Pad v7. Investigators were not blinded during all data acquisition and analysis.

## Results

### ***In vivo* and *in vitro* process of Mesenchymal-Epithelial Transition (MET): generation of secondary epithelial ovarian cancer cells (sEOC)**

Whereas EMT initiates metastasis formation by creating a mobile and migratory cancer cell phenotype, the final step in the establishment of tumors on secondary metastatic site involves the reverse process of transitioning from the mesenchymal state back to an epithelial phenotype, known as MET. In ovarian cancer, this process creates "secondary" epithelial ovarian cancer cells (sEOC). Our first objective was to develop *in vitro* and *in vivo* models that would allow us to generate sEOC cells, characterize the transition and determine in more detail their epithelial/mesenchymal status. Thus, human ovarian mesenchymal cancer cells in the form of 3D spheroids were generated from epithelial ovarian cancer cells (Supp. Fig. 1) as previously described [45] and as detailed in the Material and Methods section and depicted in Supplementary Figure 2. The generated spheroids were compact and varied in size (Fig. 1). The spheroids, without further pre-selection, were injected either s.c. (Fig. 1A) or i.p. (Fig. 1B) in athymic nude mice. I.p. injection is able to measure i.p. dissemination, which involves steps such as anoikis resistance, attachment and tumor growth. Spheroids injected s.c. formed a single solid tumor while the spheroids injected i.p. formed multiple i.p. implants comparable to carcinomatosis observed in advanced stage ovarian cancer patients. Histological evaluation of the subcutaneous tumors and the i.p.

tumors showed a morphologically epithelial phenotype by H&E (Fig. 1). These data demonstrate that independently of the location (s.c or i.p.) once mesenchymal cells implant, they acquire an epithelial morphology.

Next, we recapitulated the process *in vitro* by transferring mesenchymal spheroids grown in ultra-low attachment plates to tissue culture-treated flasks (Fig. 1C). Real-time imaging showed spheroids attach to the plate surface within 2–4h followed by outward migration of cells with fibroblast-like morphology (Fig. 1C white arrows). The cells maintained this fibroblast-like phenotype until about 48h and acquired an epithelial morphology around 72h (Fig. 1C). Thus morphologically, these *in vitro* and *in vivo* models demonstrate the occurrence of MET and the generation of sEOC as such allowing us to further characterize its molecular signature.

### **Molecular signature of sEOC is distinct from the primary epithelial ovarian cancer cells**

Our next objective was to characterize the gene expression profile of the sEOC and determine if these cells also re-acquire the epithelial molecular signature of the “primary” epithelial ovarian cancer cells from which they were derived. Thus, we performed RNA sequencing using the three primary epithelial ovarian cancer cell lines (Supp. Fig. 1), their derived mesenchymal spheroids (Fig. 1), and their corresponding sEOC (Fig. 1C and Supp. Fig. 2). Enrichment analysis by Process Networks showed that genes involved in “Development EMT regulation of epithelial to mesenchymal transition” are significantly differentially expressed between the primary epithelial ovarian cancer cells and spheroids ( $p = 0.00008$ ). Classical mesenchymal markers such as TWIST-1 and TGFB3 (marked with \*) are increased in the spheroids compared to the primary epithelial cells demonstrating the acquisition of a mesenchymal molecular signature (Fig. 2Ai). However, the molecular signature of the sEOC maintained a high degree of similarity with the mesenchymal spheroids rather than the primary epithelial ovarian cancer cells, suggesting that the original epithelial phenotype was not completely re-gained by the sEOC. Indeed, cluster analysis shows that the molecular signature of the sEOC recapitulates the signature of the mesenchymal spheroids more than the signature of the primary epithelial ovarian cancer cells (Fig. 2Aii). Validation of several epithelial markers at the protein level showed that markers originally expressed by primary epithelial cancer cells are lost in the spheroids and more importantly, not re-gained by the sEOC (Fig. 2Bi). Analysis of several mesenchymal markers showed that markers gained by spheroids are maintained by sEOC. For instance, in the OVCAR3 cell line, Keratin 18, B-catenin, and Claudin-3 are expressed by the primary epithelial cancer cells, lost in the spheroids, and not re-gained by the sEOC. In addition, compared to primary epithelial cancer cells, the OVCAR3 spheroids gained TWIST-1, FOXC2, and Vimentin (Fig. 2Bii). Interestingly, although sEOC obtained from the OVCAR3 cell line demonstrated an epithelial morphology and lower levels of FOXC2, the cells gained Slug, maintained the expression of Vimentin, and moreover showed upregulated TWIST-1 expression (Fig. 2Bii). Indeed, the upregulation of TWIST-1 in the sEOC compared to the spheroids can be observed in all the cell lines tested (Fig. 2Bii and Supp. Fig. 3). Taken together, these results demonstrate that during the formation of sEOC from mesenchymal spheroids, distinct mesenchymal markers such as FOXC2 are lost but overall, although sEOC present an epithelial morphology, it does not fully recapitulate the molecular

signature of the primary epithelial ovarian cancer cells. Of particular note is the increase in the master EMT effector TWIST-1, which remained to be highly expressed when mesenchymal spheroids differentiate into sEOC *in vitro* and upon formation of xenografts *in vivo* (Fig. 2Bii and iii).

### **TWIST-1 is upregulated but inactive in the sEOC**

To better understand the functional relevance of the observed increase in the transcription factor TWIST-1 in the sEOC [22] we measured the mRNA levels of *FOXC2* and *miR-199a*, which are two known downstream target genes of TWIST-1 [22, 45, 46, 52, 53](Fig. 3Ai). The expression of these genes was compared between the mesenchymal spheroids and sEOC. Since TWIST-1 expression is higher in sEOC than the spheroids (Fig. 2Bii and Supp. Fig. 3), the expectation was that both *FOXC2* and *miR-199a* would also be higher in the sEOC. Interestingly, qRT-PCR results showed that the two genes were significantly lower in sEOC when compared to spheroids (Fig. 3Aii) despite TWIST-1 being higher in the sEOC. This suggests that in the sEOC, TWIST-1 is not able to access the promoter region of these genes.

To validate this hypothesis we used a miR-199a promoter reporter plasmid (pGL3-miR-199a-Luc; Fig. 3Bi) which contains TWIST-1 binding sites (E-box) [46]. Co-transfection of this reporter plasmid with pcDNA-TWIST-1 in 293T cells (Fig. 3Bii) resulted in increased luminescence compared to empty vector control (Fig. 3Biii) validating the functionality of the reporter plasmid. However, transfection of pGL3-miR-199a-Luc in sEOC, which harbor abundant levels of endogenous TWIST-1 (Fig. 3Bii) demonstrated significantly lower levels of luciferase activity compared to 293T cells expressing ectopic TWIST-1 (Fig. 3Biii). These results demonstrate that indeed TWIST-1 is not able to access the promoter region of mir-199A in the sEOC. Taken together our results so far demonstrate that even though TWIST-1 is highly increased in sEOC, its transcriptional functionality is not proportionately enhanced and that regulatory mechanisms are in place in the sEOC, which control TWIST-1 transcriptional activity.

### **CBX7 inhibits TWIST-1 activity and maintains the epithelial morphology of sEOC**

Our next objective was to further investigate the mechanisms and functional significance of the discordance between TWIST-1 protein levels and its transcriptional activity in sEOC. The Polycomb Repressive Complex (PRC) is a major transcriptional regulator during cell differentiation and controls the expression and function of mesenchymal/stem cell-associated genes [31, 33]. Thus, we investigated whether there are changes in the expression of the PRC1 and PRC2 family members during the formation of sEOC from spheroids. Quantification of the different family members at the mRNA level showed most members to have increased expression in sEOC compared to spheroids with CBX7 and PCGF2, members of the PRC1 complex, as being the most differentially expressed (Fig. 4Ai [39, 40]). We then validated CBX7 expression at the protein level and as shown in Figure 4Aii, the highest expression of CBX7 was mainly observed in the sEOC, with very minimal expression in the spheroids and the primary epithelial cells. Upon validation of the increased protein expression of CBX7 in sEOC, we then determined if its knock-down (KD) would have a functional impact on the sEOC. We achieved CBX7 KD using shRNA (Fig. 4Bi) and

interestingly observed that the decrease in CBX7 in sEOC was associated with morphological changes such as the acquisition of a fibroblastic morphology, detachment from the tissue culture-treated plate, and formation of spheroids (Fig. 4Bii). This is in contrast to sEOC transfected with empty vector control, which remained to grow as a monolayer and continued to display an epithelial morphology (Fig 4Bii). These results suggest that inhibition of CBX7 expression is sufficient to push the cells towards a more mesenchymal phenotype.

We then hypothesized that this observed effect of CBX7 KD in sEOC may due to the re-activation of TWIST-1 transcriptional activity in these cells. To test this hypothesis we evaluated the mRNA levels of *miR-199a*, which as stated above is a TWIST-1 regulated gene. As shown in Figure 4Biii, KD of CBX7 in sEOC is associated with increased mRNA levels of *miR-199a*. In addition, KD of CBX7 in sEOC is associated with increased protein expression of FOXC2, another TWIST-1 target (Fig. 4Bi). No change in TWIST-1 protein expression was observed between sEOC transfected with control shRNA and those transfected with shCBX7 (data not shown). These results are indicative of the restoration of TWIST-1 activity in sEOC cells upon CBX7 KD and suggest that CBX7 can function as a break, which inhibits TWIST-1 activity.

### **CBX7 shares a common promoter-binding region with TWIST-1 and precludes TWIST-1 from the promoter**

We then determined the mechanism by which CBX7 might inhibit TWIST-1 function. First, we tested whether CBX7 could directly bind TWIST-1 (protein-protein interaction) and consequently sequester TWIST-1 to prevent it from accessing its target genes' promoters. To test this hypothesis, we immunoprecipitated (IP) TWIST-1 in sEOC and determined the presence of CBX7 in the IP complex. As shown in Supp. Fig. 4A, we did not detect CBX7 in the IP complex. Similarly, IP of CBX7 in sEOC did not show the presence of TWIST-1 (Supp. Fig. 4B) demonstrating that in sEOC, CBX7 is not bound to TWIST-1. To further confirm these results we performed the same IP assays in 293T cells transiently transfected with pcDNA-TWIST-1 and pcDNA-CBX7. Similarly, we were not able to detect the presence of CBX7 in the TWIST-1 IP complex or the presence of TWIST-1 in the CBX7 IP complex (data not shown) demonstrating that indeed CBX7 and TWIST-1 do not readily bind in cells.

Another possible mechanism by which CBX7 may prevent TWIST-1 from accessing its target genes' promoters is by binding directly to the promoter and thus precluding TWIST-1. To test this hypothesis, we determined whether CBX7 could bind to the E-box, which is the TWIST binding motif, at its target genes' promoter region. Thus, we performed chromatin immunoprecipitation (ChIP) in sEOC using a specific antibody against CBX7. The chromatin was then released from the immunocomplex and the presence of the E-box was determined by qPCR using two sets of primers that are specific for the E-box within the mir199A promoter (Fig. 5A). As shown in Figure 5B, we observed an enrichment of mir-199A promoter in the anti-CBX7 IP product compared to IgG control using both primer sets. These results demonstrate that CBX7 could bind to or close to the E-box of the promoter region of miR-199A, indicative that the presence of CBX7 precludes TWIST-1

from accessing the E-box at the promoter region consequently inhibiting TWIST-1 transcriptional activity.

To conclusively show that CBX7 can block TWIST-1 initiated transcription we performed a competitive assay in 293T cells. Cells were co-transfected with pGL3-miR-199a-Luc (containing the E-box) and pcDNA-TWIST-1 in the presence of either pcDNA-CBX7 or empty vector control (Fig. 5C). Co-transfection of pGL3-miR-199a-Luc and pcDNA-TWIST-1 showed significantly higher promoter activity compared to pGL3-miR-199a-Luc and empty pcDNA vector showing that the promoter activity is specifically coming from TWIST-1 (Fig. 5D). However, the presence of pcDNA-CBX7 significantly decreased this TWIST-1-initiated promoter activity (Fig. 5D) conclusively demonstrating that CBX7 is indeed able to inhibit TWIST-1-initiated transcription. Collectively our results demonstrate that CBX7 is able to bind the E-box and as a result preclude TWIST-1 from accessing its target gene's promoters and thus inhibiting its transcriptional activity. Thus in sEOC, the presence of CBX7 confers an epithelial phenotype against a molecular background of high TWIST-1.

### Loss of CBX7 enhances tumorigenicity and metastatic potential in sEOC

Our results thus far show the mechanism by which CBX7 can block TWIST-1 function and consequently promote an epithelial morphology even in cells with high levels of TWIST-1. To further demonstrate that the presence of CBX7 is able to block TWIST-1 function and maintain an epithelial phenotype, CBX7 was knocked-out (KO) in sEOC using CRISPR-Cas9. Figure 6Ai shows that CBX7 KO was achieved in two clones (SG-1-1 and SG-4-1) and that KO of CBX7 did not have any effect on the levels of TWIST-1 (Fig. 6Ai); therefore, we were able to establish sEOC cell lines that are TWIST-1<sup>+</sup>/CBX7<sup>-</sup>. The parental cell line and each clone were then injected i.p. in athymic nude mice and tumors were allowed to progress for 8 weeks. Necropsy at this point showed that mice inoculated with parental wild-type cells (TWIST-1<sup>+</sup>/CBX7<sup>+</sup>) developed few i.p. tumors weighing up to 0.5 g (Fig. 6Aii). In comparison, mice that were inoculated with either sEOC SG1-1 or sEOC SG-4-1 (both TWIST1<sup>+</sup>/CBX7<sup>-</sup>) had significantly heavier tumor burden compared to the parental cell line and were considerably more aggressive as demonstrated by generalized carcinomatosis (Fig. 6Aii,iii). To test whether the increase in tumor burden, which was observed in animals injected with clones sEOC SG1-1 and sEOC SG-4-1 (TWIST1<sup>+</sup>/CBX7<sup>-</sup>) is associated with reactivation of TWIST-1 function we determined the expression levels of TWIST-1 target genes, *mir-199A* and *FOXC2* in the resulting i.p. tumors. Tumors formed from clones sEOC SG1-1 and sEOC SG-4-1 had significantly increased expression of both TWIST-1 target genes, *mir-199A* and *FOXC2* compared to tumors obtained from parental cells (Fig. 6Bi and ii). Taken together, these results demonstrate that the loss of CBX7 allows the re-activation TWIST-1, which translates to increased tumorigenicity and metastatic potential in ovarian cancer cells.

### Loss of TWIST-1 reduces tumorigenicity and metastatic potential in sEOC

To further demonstrate that TWIST-1 is able to regulate the capacity of cells to form extensive carcinomatosis, TWIST-1 was stably KO in OCSC1-F2 (F2-wt) cells using CRISPR-Cas9. F2-wt cells express high levels of TWIST-1 [43] and very low levels of

CBX7 (TWIST-1<sup>high</sup>/CBX7<sup>low</sup>) when compared to primary epithelial ovarian cancer cells and sEOC (Fig. 7Ai). In addition, F2-wt cells are tumorigenic and form extensive carcinomatosis [56]. After validating the success of TWIST-1 KO (Fig. 7Ai), the parental F2-wt cell line (F2-wt) and the TWIST-1 KO clone (F2-TWKO) were inoculated i.p. in athymic nude mice. The loss of TWIST-1 had major impact on the capacity of the cells to form carcinomatosis. Quantification of tumor burden showed that animals inoculated with F2-TWKO cells had significantly less implantation sites and significantly less i.p. tumor burden compared to F2-wt (Fig. 7Aii,iii). These results demonstrate the importance of TWIST-1 expression and function and its impact on ovarian cancer tumorigenicity and metastatic potential.

Finally, to determine the impact of the loss of both TWIST-1 and CBX7 in tumor formation, we used human ovarian cancer cells that do not express endogenous TWIST-1 nor CBX7 (TWIST-1<sup>-</sup>/CBX7<sup>-</sup>) (Fig. 7Bi). I.p. injection of these cells to nude mice did not result in tumor formation (Fig. 7Bii). In contrast, carcinomatosis was observed in mice that were injected with OCSC1-F2 wild-type cells (F2-wt;TWIST-1<sup>high</sup>/CBX7<sup>low</sup>).

### Prognostic value of CBX7 and TWIST-1 in patients with ovarian cancer

Given that our data demonstrate the ability of CBX7 to inhibit the pro-mesenchymal and pro-invasiveness function of TWIST-1, we hypothesize that patients expressing CBX7 would exhibit better prognosis, especially in the context of TWIST-1 positivity. Thus, we quantified the expression of TWIST-1 and CBX7 in tumor samples obtained from patients diagnosed with ovarian cancer. We observed a varied expression pattern and intensity among the samples investigated (Fig. 8A) and were able to group the patients into 4 categories: double negative (TWIST-1<sup>neg</sup>/CBX7<sup>neg</sup>); double positive (TWIST-1<sup>pos</sup>/CBX7<sup>pos</sup>); and single positives, TWIST-1<sup>pos</sup>/CBX7<sup>neg</sup> or TWIST-1<sup>neg</sup>/CBX7<sup>pos</sup>. We then evaluated whether we can define a correlation between these four groups and clinical outcome. Survival analysis shows that TWIST-1<sup>neg</sup> patients generally do better than TWIST-1<sup>pos</sup> patients. In TWIST-1<sup>neg</sup> patients, the presence of CBX7 does not have a significant impact on survival. However, a clear separation can be observed in TWIST-1<sup>pos</sup> patients depending on whether CBX7 is co-expressed or not with TWIST-1<sup>pos</sup>/CBX7<sup>pos</sup> patients showing better overall survival than TWIST-1<sup>pos</sup>/CBX7<sup>neg</sup> (Fig. 8B). Taken together, these findings demonstrate that the absence of TWIST-1 is a positive predictor. However in the presence of TWIST-1, the co-expression of CBX7 allows further stratification of patients and identifies those with better prognosis.

## Discussion

We demonstrate in this study that despite the epithelial morphology of sEOC, these cells do not fully re-acquire the molecular signature of the primary epithelial cancer cells from which they are derived. Instead, these cells maintained a mesenchymal molecular signature. TWIST-1 expression is upregulated in these cells but its transcriptional activity is blocked by CBX7 (Supp. Fig. 5A). The transcriptional inactivity of TWIST-1, at least for the FOXC2 and mir-199A promoters, is due to competition with CBX7 on these genes' E-box. CBX7 bound at or near the E-box region prevents TWIST-1 from accessing these promoters

consequently preventing the initiation of TWIST-1 induced transcription. Loss of CBX7 was sufficient for TWIST-1 to re-gain its transcriptional activity and for sEOC to obtain a mesenchymal morphology and enhanced tumorigenicity and metastatic potential (Supp. Fig. 5B).

The persistence of TWIST-1 upon the formation of sEOC and the concomitant gain in CBX7 contributes to molecular mechanisms that confer to these cells the ease to revert from an epithelial to a mesenchymal state, and vice versa. This may contribute to the rapidly expanding intra-abdominal carcinomatosis observed during ovarian cancer progression. Indeed, our analysis of patient samples demonstrated the value of the addition of CBX7 to TWIST-1 as a marker for prognosis. Whereas CBX7 positivity does not affect overall survival in TWIST-1<sup>neg</sup> patients, the presence of CBX7 improves survival in TWIST-1<sup>pos</sup> patients, potentially by decreasing the metastatic capacity. This clinical observation ties in to the detected anti-metastatic properties of CBX7 observed in the described *in vitro* and *in vivo* studies. Based on these mechanisms we can sub-classify ovarian tumors based on the expression of CBX7 and TWIST-1 and this can be used to predict clinical outcomes and patient prognosis.

TWIST-1 is a transcription factor that is essential during development [57, 58]. Its absence is lethal to mouse embryos and its mutations cause several diseases in humans such as the Saethre-Chotzen syndrome [59–62]. During development, TWIST-1 is a robust effector of EMT and promotes this differentiation process by controlling the transcription of key regulatory genes (i.e. repression of E-cadherin, transcription of Slug, etc. [63, 64]). Interestingly, EMT induced by other effectors such as Snail and Zeb has been shown to be “moderate” when compared to TWIST-1-induced EMT[64]. The ability of TWIST-1 to promote cell mobility is a property that has been hijacked by cancer cells. Overexpression of TWIST-1 is sufficient for cancer cells to acquire a mesenchymal phenotype with enhanced migratory and invasive properties [65, 66]. In mouse models of squamous cell carcinoma, induction of Twist-1 is sufficient for cancer cells to undergo EMT and disseminate to distant sites [67]. At the distant sites however, the establishment of tumors on these secondary locations required the loss of Twist-1 function as Twist-1 negatively correlates with cell proliferation[68]. Consequently, it has been thought that the final step in cancer cell metastasis requires the process of MET, which occurs with the loss TWIST-1 transcription factor activity. Indeed, studies using patient samples have demonstrated the high expression of TWIST-1 in primary tumors and very low expression in metastatic sites [16]. Our findings suggest that in ovarian cancer, complete MET does not occur in the metastatic sites; and that the metastatic cells are in a transitional state (Supp. Fig. 5) as demonstrated by the persistence of TWIST-1 expression. The demonstration that TWIST-1 activity is essentially blocked in these cells by CBX7 showcases a novel regulation of TWIST-1 activity and demonstrates a mechanism that can maintain a transitional stage (between epithelial and mesenchymal phenotype). This regulatory mechanism conferred by CBX7 evidently presents a quicker and more robust control of TWIST-1 function as it is controlled not at the transcription level but at the protein level.

CBX7 belongs to the PcG family of proteins that make up the PRC1. Together with the PRC2, PRC1 maintains the silencing of genes required for development [69]. Specifically,

PRC1 has E3 ligase activity with CBX7 conferring the ability to bind to H3K27me3 sites and thus controlling gene expression [70]. Interestingly, CBX7 has been demonstrated to be both an oncogene [71] [72] [73], wherein together with c-Myc it promotes aggressiveness in lymphomas; and a tumor suppressor, wherein it inhibits HDAC2 in repressing the transcription of the gene that codes for E-cadherin [74, 75]. Seminal work by Forzati et al established CBX7 as a tumor suppressor as its ablation leads to the development of liver and lung adenocarcinomas [72, 76]. CBX7 has since been demonstrated to be inversely correlated with tumor stage, malignant grade, aggressiveness, and patient survival in multiple tumor types [70, 77]. In our studies, CBX7-induced regulation of TWIST-1 activity allows the acquisition of an epithelial morphology in the setting of high levels of TWIST-1. This regulatory network results in a molecular mechanism that can be promptly overturned by the loss of CBX7 leading to the acquisition of mesenchymal phenotype and enhanced tumorigenic potential, which may explain the rapid disease progression and dissemination observed in ovarian cancer patients. A well-known mechanism that controls CBX7 expression are microRNA's [78, 79] and on-going studies in our lab are trying to determine key stimuli in the ovarian tumor microenvironment that can lead to the loss of CBX7 in secondary metastatic sites.

In conclusion we demonstrate that mesenchymal ovarian cancer cells do not undergo complete MET in the secondary sites. Although sEOC display an epithelial morphology, they do not re-gain the full epithelial molecular signature of the primary epithelial ovarian cancer cells from which they were derived. Instead, sEOC maintain high levels of TWIST-1 whose activity is blocked by CBX7 (Supp. Fig. 5A). This regulation allows secondary tumors to achieve an epithelial morphology while maintaining the expression of TWIST-1 and confers an advantage of prompt reversal to a mesenchymal morphology and gain in tumorigenic potential upon perturbation of CBX7 (Supp. Fig. 5B). This may explain the rapid progression of metastasis in ovarian cancer patients. More importantly, based on this regulatory mechanism we can sub-classify ovarian tumors based on CBX7 and TWIST-1 positivity and this can be used to predict clinical outcomes.

## Supplementary Material

Refer to Web version on PubMed Central for supplementary material.

## Acknowledgement:

This study is supported in part by grants from NIH NCI R01CA199004 (GM), The National Natural Science Foundation of China No. 81572900 (GY), The National Key R&D Program of China, Stem Cell and Translation Research No. 2016YFA0102000 (GY), and Hunan Provincial Natural Science Foundation of China No. 2018JJ3820 (JL).

## References

1. Hildreth NG, Kelsey JL, LiVolsi VA, Fischer DB, Holford TR, Mostow ED et al. An epidemiologic study of epithelial carcinoma of the ovary. *Am J Epidemiol* 1981; 114: 398–405. [PubMed: 7304575]
2. Heintz AP, Odicino F, Maisonneuve P, Quinn MA, Benedet JL, Creasman WT et al. Carcinoma of the ovary. FIGO 26th Annual Report on the Results of Treatment in Gynecological Cancer.

International journal of gynaecology and obstetrics: the official organ of the International Federation of Gynaecology and Obstetrics 2006; 95 Suppl 1: S161–192.

3. Goff BA, Balas C, Tenenbaum C. Ovarian cancer national alliance: A report of the 2012 Consensus Conference on Current Challenges in ovarian cancer. *Gynecol Oncol* 2013.
4. Kurman RJ, Shih Ie M. The origin and pathogenesis of epithelial ovarian cancer: a proposed unifying theory. *Am J Surg Pathol* 2010; 34: 433–443. [PubMed: 20154587]
5. Thrall MM, Gray HJ, Symons RG, Weiss NS, Flum DR, Goff BA. Trends in treatment of advanced epithelial ovarian cancer in the Medicare population. *Gynecol Oncol* 2011; 122: 100–106. [PubMed: 21496889]
6. Armstrong DK. Relapsed ovarian cancer: challenges and management strategies for a chronic disease. *Oncologist* 2002; 7 Suppl 5: 20–28.
7. Jelovac D, Armstrong DK. Recent progress in the diagnosis and treatment of ovarian cancer. *CA Cancer J Clin* 2011; 61: 183–203. [PubMed: 21521830]
8. Jarboe EA, Folkins AK, Drapkin R, Ince TA, Agoston ES, Crum CP. Tubal and ovarian pathways to pelvic epithelial cancer: a pathological perspective. *Histopathology* 2008; 53: 127–138. [PubMed: 18298580]
9. Naora H, Montell DJ. Ovarian cancer metastasis: integrating insights from disparate model organisms. *Nat Rev Cancer* 2005; 5: 355–366. [PubMed: 15864277]
10. Singh A, Settleman J. EMT, cancer stem cells and drug resistance: an emerging axis of evil in the war on cancer. *Oncogene* 2010; 29: 4741–4751. [PubMed: 20531305]
11. Tan TZ, Miow QH, Miki Y, Noda T, Mori S, Huang RY et al. Epithelial-mesenchymal transition spectrum quantification and its efficacy in deciphering survival and drug responses of cancer patients. *EMBO molecular medicine* 2014; 6: 1279–1293. [PubMed: 25214461]
12. Vergara D, Merlot B, Lucot JP, Collinet P, Vinatier D, Fournier I et al. Epithelial-mesenchymal transition in ovarian cancer. *Cancer Lett* 2010; 291: 59–66. [PubMed: 19880243]
13. Chen R, Alvero AB, Silasi DA, Steffensen KD, Mor G. Cancers take their Toll--the function and regulation of Toll-like receptors in cancer cells. *Oncogene* 2008; 27: 225–233. [PubMed: 18176604]
14. Ye X, Weinberg RA. Epithelial-Mesenchymal Plasticity: A Central Regulator of Cancer Progression. *Trends in cell biology* 2015; 25: 675–686. [PubMed: 26437589]
15. Zeisberg M, Neilson EG. Biomarkers for epithelial-mesenchymal transitions. *Journal of Clinical Investigation* 2009; 119: 1429–1437376.
16. Zheng X, Carstens JL, Kim J, Scheible M, Kaye J, Sugimoto H et al. Epithelial-to-mesenchymal transition is dispensable for metastasis but induces chemoresistance in pancreatic cancer. *Nature* 2015; 527: 525–530. [PubMed: 26560028]
17. Jolly MK, Ware KE, Gilja S, Somarelli JA, Levine H. EMT and MET: necessary or permissive for metastasis? *Mol Oncol* 2017; 11: 755–769. [PubMed: 28548345]
18. Yao D, Dai C, Peng S. Mechanism of the mesenchymal-epithelial transition and its relationship with metastatic tumor formation. *Mol Cancer Res* 2011; 9: 1608–1620. [PubMed: 21840933]
19. Jordan NV, Johnson GL, Abell AN. Tracking the intermediate stages of epithelial-mesenchymal transition in epithelial stem cells and cancer. *Cell Cycle* 2011; 10: 2865–2873. [PubMed: 21862874]
20. Lovisa S, LeBleu VS, Tampe B, Sugimoto H, Vadrnagara K, Carstens JL et al. Epithelial-to-mesenchymal transition induces cell cycle arrest and parenchymal damage in renal fibrosis. *Nat Med* 2015; 21: 998–1009. [PubMed: 26236991]
21. Ansieau S, Bastid J, Doreau A, Morel AP, Bouchet BP, Thomas C et al. Induction of EMT by twist proteins as a collateral effect of tumor-promoting inactivation of premature senescence. *Cancer Cell* 2008; 14: 79–89. [PubMed: 18598946]
22. Yin G, Chen R, Alvero AB, Fu HH, Holmberg J, Glackin C et al. TWISTing stemness, inflammation and proliferation of epithelial ovarian cancer cells through MIR199A2/214. *Oncogene* 2010; 29: 3545–3553. [PubMed: 20400975]
23. Glackin C, Winters K, Murray E, Murray S. Transcripts encoding the basic-helix-loop-helix factor twist are expressed in mouse embryos, cell lines, and adult tissues. *Mol Cell Differ* 1994; 2: 309–328.

24. Carmona-Fontaine C, Theveneau E, Tzekou A, Tada M, Woods M, Page KM et al. Complement fragment C3a controls mutual cell attraction during collective cell migration. *Dev Cell* 2011; 21: 1026–1037. [PubMed: 22118769]
25. Comijn J, Berx G, Vermassen P, Verschueren K, van Grunsven L, Bruyneel E et al. The two-handed E box binding zinc finger protein SIP1 downregulates E-cadherin and induces invasion. *Mol Cell* 2001; 7: 1267–1278. [PubMed: 11430829]
26. Fabregat I, Malfettone A, Soukupova J. New Insights into the Crossroads between EMT and Stemness in the Context of Cancer. *Journal of clinical medicine* 2016; 5. [PubMed: 28465746]
27. Willert K, Brown JD, Danenberg E, Duncan AW, Weissman IL, Reya T et al. Wnt proteins are lipid-modified and can act as stem cell growth factors. *Nature* 2003; 423: 448–452. [PubMed: 12717451]
28. Gomez Tejada Zanudo J, Guinn MT, Farquhar K, Szenk M, Steinway SN, Balazsi G et al. Towards control of cellular decision-making networks in the epithelial-to-mesenchymal transition. *Phys Biol* 2019; 16: 031002.
29. Kian W, Roisman LC, Peled N. Two are better than one on progression through MET mechanism for EGFR+ NSCLC patients. *Transl Lung Cancer Res* 2018; 7: S334–s335. [PubMed: 30705848]
30. Yao D, Peng S, Dai C. The role of hepatocyte nuclear factor 4alpha in metastatic tumor formation of hepatocellular carcinoma and its close relationship with the mesenchymal-epithelial transition markers. *BMC cancer* 2013; 13: 432. [PubMed: 24059685]
31. Leeb M, Pasini D, Novatchkova M, Jaritz M, Helin K, Wutz A. Polycomb complexes act redundantly to repress genomic repeats and genes. *Genes & development (Research Support, Non-U.S. Gov't)* 2010; 24: 265–276.
32. Leeb M, Wutz A. Polycomb complexes - Genes make sense of host defense. *Cell Cycle (Editorial)* 2010; 9: 2692–2693.
33. Margueron R, Reinberg D. The Polycomb complex PRC2 and its mark in life. *Nature (Research Support, N.I.H., Extramural, Research Support, Non-U.S. Gov't, Review)* 2011; 469: 343–349.
34. Morey L, Helin K. Polycomb group protein-mediated repression of transcription. *Trends in biochemical sciences (Research Support, Non-U.S. Gov't, Review)* 2010; 35: 323–332.
35. Alvero AB, Chen R, Fu HH, Montagna M, Schwartz PE, Rutherford T et al. Molecular phenotyping of human ovarian cancer stem cells unravels the mechanisms for repair and chemoresistance. *Cell Cycle* 2009; 8: 158–166. [PubMed: 19158483]
36. Alvero AB, Montagna MK, Chen R, Kim KH, Kyungjin K, Visintin I et al. NV-128, a novel isoflavone derivative, induces caspase-independent cell death through the Akt/mammalian target of rapamycin pathway. *Cancer* 2009; 115: 3204–3216. [PubMed: 19472400]
37. Alvero AB, O'Malley D, Brown D, Kelly G, Garg M, Chen W et al. Molecular mechanism of phenoxodiol-induced apoptosis in ovarian carcinoma cells. *Cancer* 2006; 106: 599–608. [PubMed: 16388521]
38. Cardenas C, Montagna MK, Pitruzzello M, Lima E, Mor G, Alvero AB. Adipocyte microenvironment promotes Bclxl expression and confers chemoresistance in ovarian cancer cells. *Apoptosis* 2017; 22: 558–569. [PubMed: 28012060]
39. Kelly MG, Alvero AB, Chen R, Silasi DA, Abrahams VM, Chan S et al. TLR-4 signaling promotes tumor growth and paclitaxel chemoresistance in ovarian cancer. *Cancer Res* 2006; 66: 3859–3868. [PubMed: 16585214]
40. Yang-Hartwich Y, Tedja R, Roberts CM, Goodner-Bingham J, Cardenas C, Gurea M et al. p53-Pirh2 Complex Promotes Twist1 Degradation and Inhibits EMT. *Mol Cancer Res* 2019; 17: 153–164. [PubMed: 30131448]
41. Alvero AB, Heaton A, Lima E, Pitruzzello M, Sumi N, Yang-Hartwich Y et al. TRX-E-002-1 Induces c-Jun-Dependent Apoptosis in Ovarian Cancer Stem Cells and Prevents Recurrence In Vivo. *Mol Cancer Ther* 2016; 15: 1279–1290. [PubMed: 27196760]
42. Alvero AB, Kim D, Lima E, Sumi NJ, Lee JS, Cardenas C et al. Novel approach for the detection of intraperitoneal micrometastasis using an ovarian cancer mouse model. *Sci Rep* 2017; 7: 40989. [PubMed: 28120873]

43. Craveiro V, Yang-Hartwich Y, Holmberg JC, Joo WD, Sumi NJ, Pizzonia J et al. Phenotypic modifications in ovarian cancer stem cells following Paclitaxel treatment. *Cancer Med* 2013; 2: 751–762. [PubMed: 24403249]
44. Pizzonia J, Holmberg J, Orton S, Alvero A, Viteri O, McLaughlin W et al. Multimodality animal rotation imaging system (Mars) for in vivo detection of intraperitoneal tumors. *Am J Reprod Immunol* 2012; 67: 84–90. [PubMed: 21951577]
45. Yin G, Alvero AB, Craveiro V, Holmberg JC, Fu HH, Montagna MK et al. Constitutive proteasomal degradation of TWIST-1 in epithelial-ovarian cancer stem cells impacts differentiation and metastatic potential. *Oncogene* 2013; 32: 39–49. [PubMed: 22349827]
46. Lee YB, Bantounas I, Lee DY, Phylactou L, Caldwell MA, Uney JB. Twist-1 regulates the miR-199a/214 cluster during development. *Nucleic Acids Res* 2009; 37: 123–128. [PubMed: 19029138]
47. Kamsteeg M, Rutherford T, Sapi E, Hanczaruk B, Shahabi S, Flick M et al. Phenoxodiol--an isoflavone analog--induces apoptosis in chemoresistant ovarian cancer cells. *Oncogene* 2003; 22: 2611–2620. [PubMed: 12730675]
48. Tedja R, Roberts CM, Alvero AB, Cardenas C, Yang-Hartwich Y, Spadinger S et al. Protein kinase Calpha-mediated phosphorylation of Twist1 at Ser-144 prevents Twist1 ubiquitination and stabilizes it. *J Biol Chem* 2019; 294: 5082–5093. [PubMed: 30733340]
49. Yang-Hartwich Y, Soteras MG, Lin ZP, Holmberg J, Sumi N, Craveiro V et al. p53 protein aggregation promotes platinum resistance in ovarian cancer. *Oncogene* 2015; 34: 3605–3616. [PubMed: 25263447]
50. Alvero AB, Montagna MK, Sumi NJ, Joo WD, Graham E, Mor G. Multiple blocks in the engagement of oxidative phosphorylation in putative ovarian cancer stem cells: implication for maintenance therapy with glycolysis inhibitors. *Oncotarget* 2014; 5: 8703–8715. [PubMed: 25237928]
51. Ran FA, Hsu PD, Wright J, Agarwala V, Scott DA, Zhang F. Genome engineering using the CRISPR-Cas9 system. *Nat Protoc* 2013; 8: 2281–2308. [PubMed: 24157548]
52. Cheng GZ, Zhang WZ, Sun M, Wang Q, Coppola D, Mansour M et al. Twist is transcriptionally induced by activation of STAT3 and mediates STAT3 oncogenic function. *The Journal of Biological Chemistry* 2008; 283: 14665–14673. [PubMed: 18353781]
53. Chen R, Alvero AB, Silasi DA, Kelly MG, Fest S, Visintin I et al. Regulation of IKKbeta by miR-199a affects NF-kappaB activity in ovarian cancer cells. *Oncogene* 2008; 27: 4712–4723. [PubMed: 18408758]
54. Duan RS, Tang GB, Du HZ, Hu YW, Liu PP, Xu YJ et al. Polycomb protein family member CBX7 regulates intrinsic axon growth and regeneration. *Cell Death Differ* 2018; 25: 1598–1611. [PubMed: 29459770]
55. Federico A, Sepe R, Cozzolino F, Piccolo C, Iannone C, Iacobucci I et al. The complex CBX7-PRMT1 has a critical role in regulating E-cadherin gene expression and cell migration. *Biochim Biophys Acta Gene Regul Mech* 2019; 1862: 509–521. [PubMed: 30826432]
56. Craveiro V, Yang-Hartwich Y, Holmberg JC, Sumi NJ, Pizzonia J, Griffin B et al. Phenotypic modifications in ovarian cancer stem cells following Paclitaxel treatment. *Cancer Medicine* 2013; 2: 751–762. [PubMed: 24403249]
57. Baylies MK, Bate M. twist: a myogenic switch in *Drosophila*. *Science* 1996; 272: 1481–1484. [PubMed: 8633240]
58. Bialek P, Kern B, Yang X, Schrock M, Sasic D, Hong N et al. A twist code determines the onset of osteoblast differentiation. *Dev Cell* 2004; 6: 423–435. [PubMed: 15030764]
59. Seto ML, Lee SJ, Sze RW, Cunningham ML. Another TWIST on Baller-Gerold syndrome. *Am J Med Genet (Case Reports, Research Support, Non-U.S. Gov't, Research Support, U.S. Gov't, P.H.S. Review)* 2001; 104: 323–330.
60. Howard TD, Paznekas WA, Green ED, Chiang LC, Ma N, Ortiz de Luna RI et al. Mutations in TWIST, a basic helix-loop-helix transcription factor, in Saethre-Chotzen syndrome. *Nat Genet (Research Support, Non-U.S. Gov't, Research Support, U.S. Gov't, P.H.S.)* 1997; 15: 36–41.
61. Glackin CA. Targeting the Twist and Wnt signaling pathways in metastatic breast cancer. *Maturitas* 2014; 79: 48–51. [PubMed: 25086726]

62. Glackin CA, Murray EJ, Murray SS. Doxorubicin inhibits differentiation and enhances expression of the helix-loop-helix genes Id and mTwi in mouse osteoblastic cells. *Biochemistry international* 1992; 28: 67–75. [PubMed: 1280141]
63. Yang J, Mani SA, Donaher JL, Ramaswamy S, Itzykson RA, Come C et al. Twist, a master regulator of morphogenesis, plays an essential role in tumor metastasis. *Cell* 2004; 117: 927–939. [PubMed: 15210113]
64. Yang MH, Hsu DS, Wang HW, Wang HJ, Lan HY, Yang WH et al. Bmi1 is essential in Twist1-induced epithelial-mesenchymal transition. *Nat Cell Biol (Research Support, Non-U.S. Gov't)* 2010; 12: 982–992.
65. Shen CH, Wu JD, Jou YC, Cheng MC, Lin CT, Chen PC et al. The correlation between TWIST, E-cadherin, and beta-catenin in human bladder cancer. *Journal of BUON : official journal of the Balkan Union of Oncology (Research Support, Non-U.S. Gov't)* 2011; 16: 733–737.
66. Yang MH, Wu MZ, Chiou SH, Chen PM, Chang SY, Liu CJ et al. Direct regulation of TWIST by HIF-1alpha promotes metastasis. *Nat Cell Biol* 2008; 10: 295–305. [PubMed: 18297062]
67. Yuen HF, Chan YP, Wong ML, Kwok WK, Chan KK, Lee PY et al. Upregulation of Twist in oesophageal squamous cell carcinoma is associated with neoplastic transformation and distant metastasis. *J Clin Pathol* 2007; 60: 510–514. [PubMed: 16822877]
68. Tsai JH, Donaher JL, Murphy DA, Chau S, Yang J. Spatiotemporal regulation of epithelial-mesenchymal transition is essential for squamous cell carcinoma metastasis. *Cancer Cell* 2012; 22: 725–736. [PubMed: 23201165]
69. Mas G, Di Croce L. The role of Polycomb in stem cell genome architecture. *Curr Opin Cell Biol* 2016; 43: 87–95. [PubMed: 27690123]
70. Pallante P, Forzati F, Federico A, Arra C, Fusco A. Polycomb protein family member CBX7 plays a critical role in cancer progression. *Am J Cancer Res* 2015; 5: 1594–1601. [PubMed: 26175930]
71. Scott CL, Gil J, Hernando E, Teruya-Feldstein J, Narita M, Martinez D et al. Role of the chromobox protein CBX7 in lymphomagenesis. *Proc Natl Acad Sci U S A* 2007; 104: 5389–5394. [PubMed: 17374722]
72. Forzati F, Federico A, Pallante P, Abbate A, Esposito F, Malapelle U et al. CBX7 is a tumor suppressor in mice and humans. *J Clin Invest* 2012; 122: 612–623. [PubMed: 22214847]
73. Bernard D, Martinez-Leal JF, Rizzo S, Martinez D, Hudson D, Visakorpi T et al. CBX7 controls the growth of normal and tumor-derived prostate cells by repressing the Ink4a/Arf locus. *Oncogene* 2005; 24: 5543–5551. [PubMed: 15897876]
74. Bao Z, Xu X, Liu Y, Chao H, Lin C, Li Z et al. CBX7 negatively regulates migration and invasion in glioma via Wnt/beta-catenin pathway inactivation. *Oncotarget* 2017; 8: 39048–39063. [PubMed: 28388562]
75. Pallante P, Sepe R, Federico A, Forzati F, Bianco M, Fusco A. CBX7 modulates the expression of genes critical for cancer progression. *PLoS One* 2014; 9: e98295.
76. Forzati F, Federico A, Pallante P, Colamaio M, Esposito F, Sepe R et al. CBX7 gene expression plays a negative role in adipocyte cell growth and differentiation. *Biol Open* 2014; 3: 871–879. [PubMed: 25190058]
77. Forzati F, Federico A, Pallante P, Fedele M, Fusco A. Tumor suppressor activity of CBX7 in lung carcinogenesis. *Cell Cycle* 2012; 11: 1888–1891. [PubMed: 22544325]
78. Wu W, Zhou X, Yu T, Bao Z, Zhi T, Jiang K et al. The malignancy of miR-18a in human glioblastoma via directly targeting CBX7. *Am J Cancer Res* 2017; 7: 64–76. [PubMed: 28123848]
79. Yongyu Z, Lewei Y, Jian L, Yuqin S. MicroRNA-18a targets IRF2 and CBX7 to promote cell proliferation in hepatocellular carcinoma. *Oncol Res* 2018.

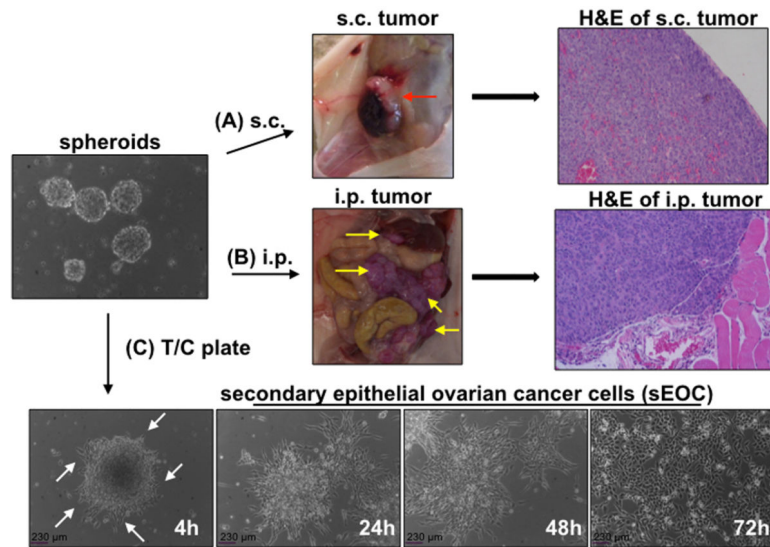


**Figure 1. Derivation of secondary epithelial ovarian cancer cells (sEOC) *in vivo* and *in vitro*.** Spheroids obtained from epithelial ovarian cancer cell lines (detailed in the Materials and Methods section) and grown in ultra-low attachment plates were injected (A) subcutaneously (s.c.) or (B) intra-peritoneally (i.p.) in athymic nude mice and resulting tumors (after 8 weeks for s.c. model and after 3 weeks for i.p. model) were stained with H&E. Red arrow points to s.c. tumor formed and yellow arrows point to i.p. tumors. Spheroids were also transferred to tissue culture-treated plates (C) and their attachment and growth catalogued. Note cellular outgrowths from the spheroids at the 4h time-point (white arrows) and the cultures' monolayer growth and epithelial morphology by the 72h time-point.

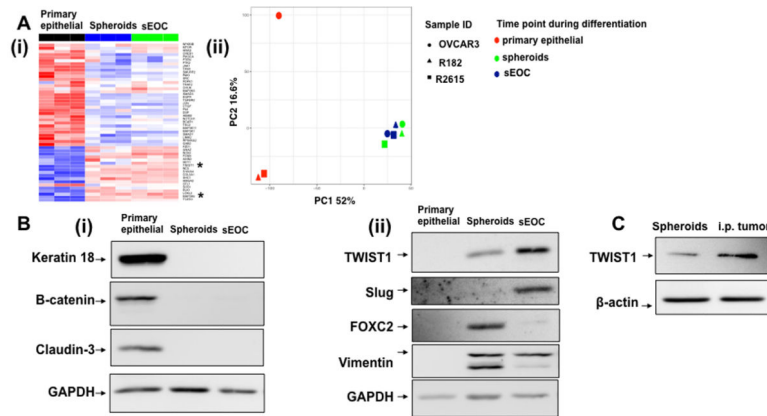


**Figure 2. sEOC is molecularly distinct from the primary epithelial ovarian cancer cells.** Three epithelial ovarian cancer cell lines (detailed in the Materials and Methods section and designated in text as primary epithelial ovarian cancer), their derived spheroids and corresponding sEOC were subjected to RNA sequencing. **(A) i**, Heat map from enrichment analysis by Process Network: “Development EMT regulation of epithelial to mesenchymal transition” showing that sEOC do not re-acquire the molecular signature of the primary epithelial ovarian cancer cells; for each phenotype (i.e. primary epithelial, spheroids, sEOC), the three columns are results for R182, R2615, and OVCAR3, respectively; each cell line was sequenced once; **ii**, Principal component analysis showing that sEOC have more variance when compared to primary epithelial ovarian cancer cells than when compared to the spheroids. **(B)** The expression of EMT markers were validated in the OVCAR3 cell lines by western blot analysis. Expression of epithelial markers **(i)** and mesenchymal markers **(ii)** were determined in primary epithelial cells, spheroids, and sEOC. **(C)** Expression of TWIST-1 protein is compared between spheroids obtained from the R182 cell line and the resulting i.p. tumor.

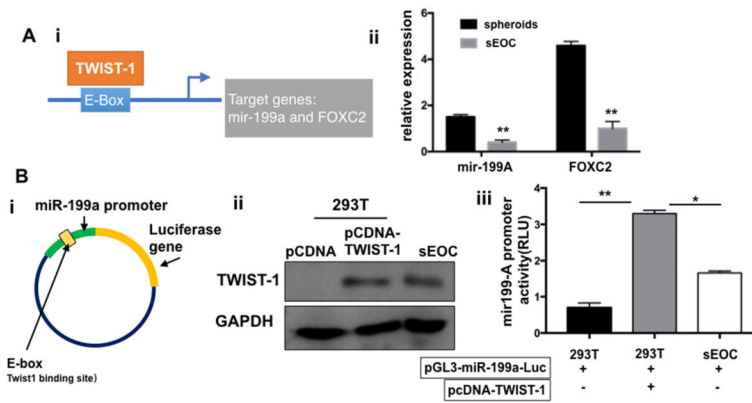


**Figure 3. TWIST-1 is inactive in the sEOC.**

(A) **i**, Depiction of E-box, the promoter element recognized by TWIST-1; **ii**, RT-qPCR analysis of TWIST-1 target genes, *mir-199A* and *FOXC2*, showing significantly lower levels in sEOC compared to spheroids, \*\*  $p < 0.01$  by unpaired student's *t* test; (B) **i**, Map of mir-199A reporter plasmid; **ii**, Western blot analyses showing levels of ectopically expressed TWIST-1 in 293T cells and endogenously expressed TWIST-1 in R182 sEOC; **iii**, 293T cells were transiently transfected with pGL3-miR-199a-Luc and pCDNA-TWIST-1 or pGL3-miR-199a-Luc and empty vector control and activity of ectopically expressed TWIST-1 on mir-199A promoter was quantified by measuring luminescence; R182 sEOC cells were transiently transfected with pGL3-miR-199a-Luc and activity of endogenously expressed TWIST-1 on mir-199A promoter was also quantified, \*  $p < 0.05$ , \*\*  $p < 0.01$  by unpaired student's *t* test.

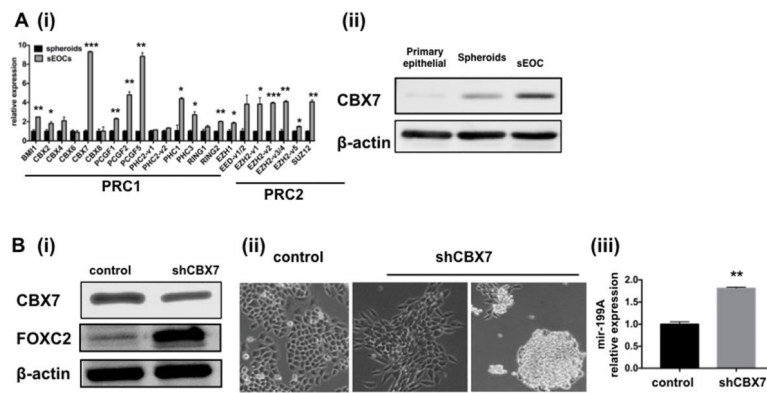


**Figure 4. Loss of CBX7 in sEOC is sufficient to promote a mesenchymal phenotype and induce TWIST-1 target genes.**

(A) **i**, RT-qPCR data showing that specific PcG proteins that make up PRC1 and PRC2 are differentially expressed in spheroids and R182 sEOC, \*  $p < 0.05$ , \*\*  $p < 0.01$ , \*\*\*  $p < 0.001$ ; **ii**, Upregulation of the PcG protein, CBX7 in R182 sEOC is confirmed at the protein level by western blot analysis; (B) **i**, CBX7 was stably knocked-down in sEOC using shRNA and effect on the TWIST-1 target, FOXC2 was determined by western blot; **ii**, KD of CBX7 in R182 sEOC leads to acquisition of a mesenchymal phenotype and **iii**, higher levels of *mir-199A* transcript, \*\*  $p = 0.004$  shCBX7 vs control by unpaired student's *t* test.

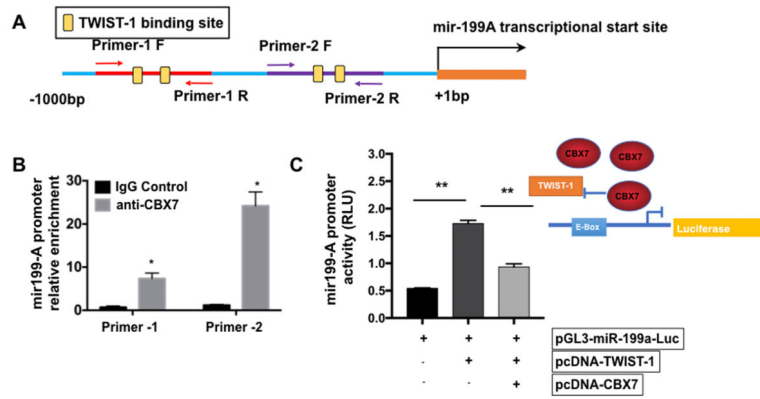


**Figure 5. CBX7 binds to mir-199A promoter region at or near the TWIST-1 binding site.** (A) Schematic diagram showing the location of the primers used within the mir-199A promoter region; (B) CBX7 was chromatin-immunoprecipitated in R182 sEOC and presence of mir-199A promoter region determined by PCR using primers in A, \*\*  $p < 0.01$ ; (C) 293T cells were transiently transfected with the described combination of plasmids and TWIST-1 activity on the mir-199A promoter was determined by measuring luminescence, \*\*  $p < 0.001$  by One way ANOVA with *post hoc* analysis.

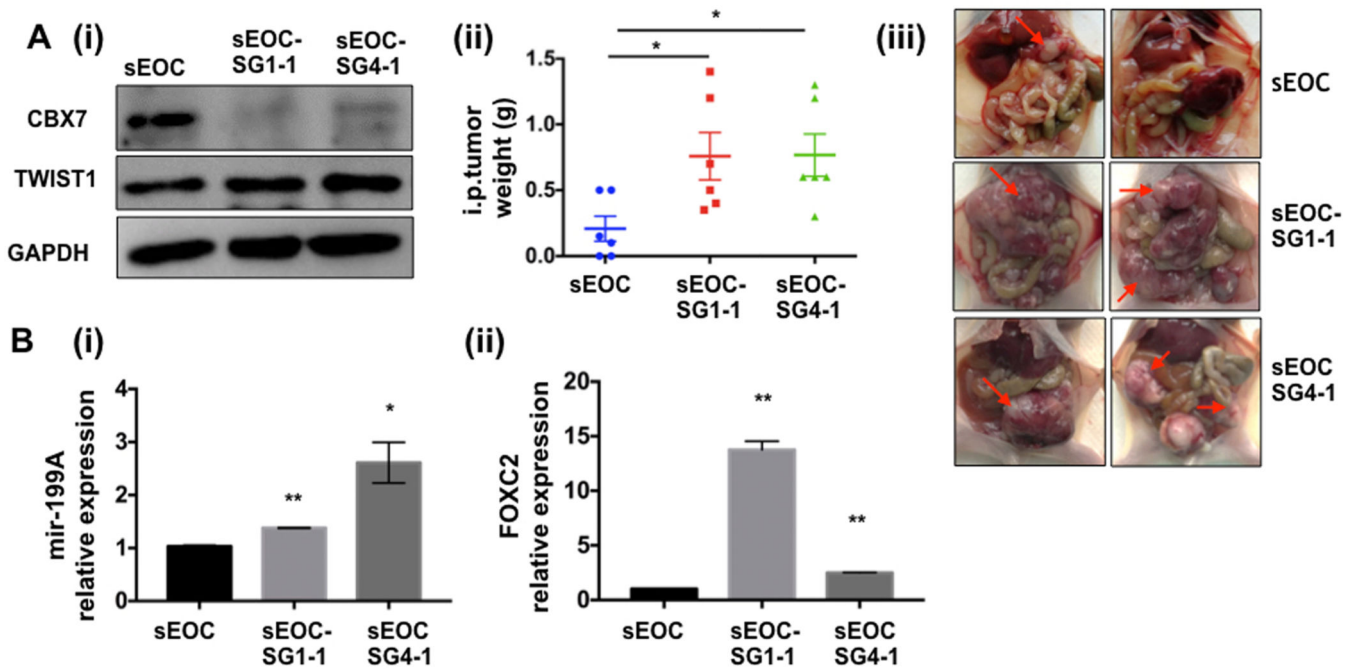


**Figure 6. Loss of CBX7 leads to enhanced metastatic potential and enhanced TWIST-1 activity *in vivo*.**

(A) **i**, CBX7 was KO in R182 sEOC using CRISPR-Cas9. The parental cell line and two KO clones (sEOC-SG1-1 and sEOC-SG1-4) were injected i.p. in athymic nude mice; **ii**, Animals were sacrificed after 8 weeks and tumor implants were dissected and, \* p < 0.05; **iii**, Gross morphology of i.p. tumors formed; two representative animals are shown per group; red arrows point to i.p. tumors; (B) **i**, *mir-199A* transcript was quantified in the resulting i.p. tumors by RT-qPCR, \* p < 0.05, \*\* p < 0.01 compared to sEOC analyzed by unpaired student's *t* test; **ii**, *FOXC2* transcript was quantified in the resulting i.p. tumors by RT-qPCR, \*\* p < 0.01 compared to sEOC analyzed by unpaired student's *t* test.

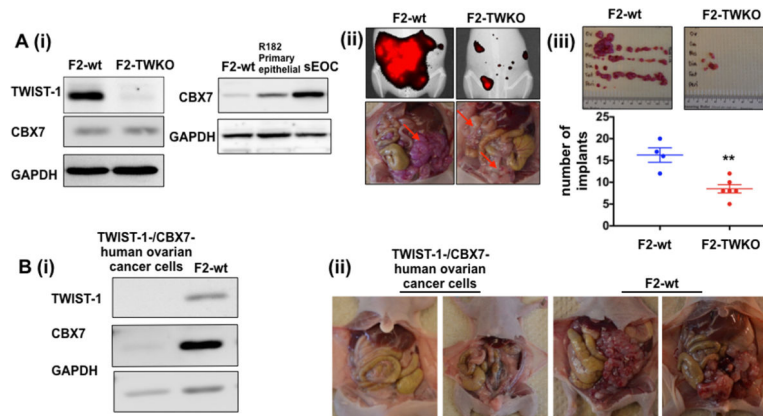


**Figure 7. Loss of TWIST-1 leads to decreased metastatic potential.**

**(A) i**, TWIST-1 was KO in mCherry<sup>+</sup>/TWIST-1<sup>high</sup>/CBX7<sup>low</sup> OCSC1-F2 ovarian cancer cells using CRISPR-Cas9; **ii**, The parental cell line (F2-wt) and KO clone (F2-TWKO) were injected i.p. in athymic nude mice and tumor progression was followed for 8 weeks; *top panel* shows fluorescence imaging at end of study and *bottom panel* shows necropsy images from representative animals; red arrows point to i.p. tumors; **iii**, I.p. tumors were dissected and separated by location, *ov*, ovarian; *om*, omental; *mes*, mesentery; *dia*, diaphragm; *fat*, omental implant; *peri*, implants on peritoneal lining; and number of implants were quantified and graphed, \*\* p < 0.01 compared to wt analyzed by unpaired student's *t* test; **(B) i**, TWIST-1<sup>-</sup>/CBX7<sup>-</sup> human ovarian cancer cells (n = 10) and mCherry<sup>+</sup>/TWIST-1<sup>high</sup>/CBX7<sup>low</sup> OCSC1-F2 (F2 wt) were injected i.p. in athymic nude mice and tumor burden evaluated; **ii**, necropsy was performed after 33 days; note the absence of i.p. tumors in TWIST-1<sup>-</sup>/CBX7<sup>-</sup> human ovarian cancer cells and the carcinomatosis formed by mCherry<sup>+</sup>/TWIST-1<sup>high</sup>/CBX7<sup>low</sup> OCSC1-F2 cells (F2-wt).

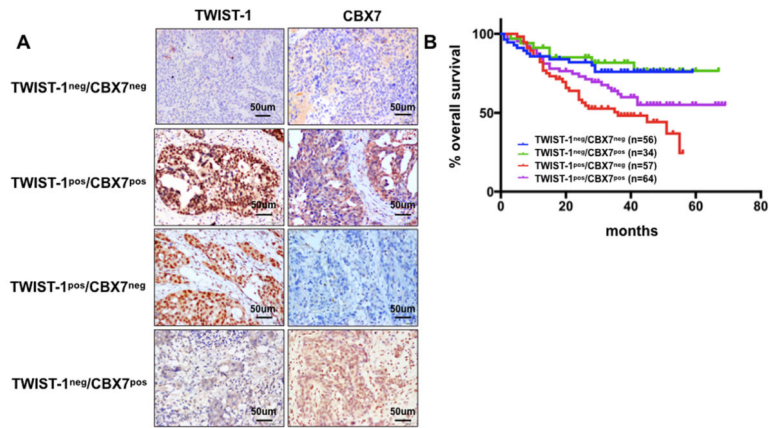


**Figure 8. CBX7 is positive predictor of survival in TWIST-1<sup>pos</sup> patients.**

Patient tumor samples were immunostained for TWIST-1 or CBX7 and classified into four groups: TWIST-1<sup>neg</sup>/CBX7<sup>neg</sup>, TWIST-1<sup>pos</sup>/CBX7<sup>pos</sup>, TWIST-1<sup>pos</sup>/CBX7<sup>neg</sup>, and TWIST-1<sup>neg</sup>/CBX7<sup>pos</sup>. **(A)** Representative images of patient staining for each group; **(B)** Kaplan Meier survival plot based on expression of TWIST-1 and CBX7 showing that in TWIST-1<sup>pos</sup> patients, the presence of CBX7 improves outcome,  $p = 0.0024$ .